AIMS Materials Science, 5(3): 414–421.
DOI: 10.3934/matersci.2018.3.414
Received: 15 February 2018
Accepted: 22 April 2018
Published: 28 April 2018

http://www.aimspress.com/journal/Materials

Research article

Electrophoresis-induced structural changes at cement-steel interface

Alexandre Lavrov[1],*, Elvia Anabela Chavez Panduro[2], Kamila Gawel[1] and Malin Torsæter[1]

[1] SINTEF, Trondheim, Norway
[2] Physics Department, Norwegian University of Science and Technology, Trondheim, Norway

*** Correspondence:** Email: alexandre.lavrov@sintef.no; Tel: +4798286658.

Abstract: Applying positive potential to a steel electrode immersed into a cement changes the packing of cement particles in the vicinity of the electrode surface. The electrophoresis-induced packing enhancement at anode has promising applications in oil & gas and CO_2 storage industries since it could be used to improve the mechanical and hydraulic cement-casing bonding in wells and thereby improve the well integrity, both in short and long term. In this experimental study, we use synchrotron radiation microtomography (μ-CT) and X-ray diffraction (XRD) analyses of the interfacial transition zone (ITZ, a 20–100 μm wide near-wall zone depleted of large particles) to find out what structural changes are responsible for different cement-steel adhesion at anode and cathode. Particle size distribution analysis reveals that the ITZ is enriched with large (equivalent diameter > 10 μm) cement particles near anode. On the contrary, near cathode, cement is depleted of large particles, which results in poor adhesion to the electrode. XRD analysis reveals that cement near anode is enriched with tricalcium silicate (Ca_3SiO_5). These findings suggest that electrophoresis-enhanced cement-steel adhesion is due to large (>10 μm) negatively-charged tricalcium silicate particles being attracted to anode.

Keywords: cement; electrophoresis; cement-steel interface; particles; interfacial transition zone (ITZ); synchrotron radiation microtomography; experiment

1. Introduction

Mechanical and hydraulic bonding strength between cement and steel is an important parameter that affects the choice of cement composition and cementing procedures in many engineering applications. Cement-steel interfaces are ubiquitous in civil engineering (e.g., interfaces between reinforcement and cement in reinforced concrete) and mining and tunnel engineering (e.g., interfaces

between rockbolts and the cement surrounding them). In oil and gas, geothermal, and CO_2 storage industries cement is used extensively in well construction to fill the annular space between the borehole wall and casing [1]. The latter is a steel pipe installed in the wellbore to prevent the surrounding rock from falling into the wellbore while the wellbore is drilled and, afterwards, when it is used for production or injection of fluids. The purpose of cementing the casing is to hold it in place, to prevent the rock from moving onto the casing, to prevent the influx of corrosive formation fluids towards the casing, and to ensure zonal isolation. The latter means that formation fluids should not be able to travel freely along the annulus between the casing and the rock. Poor bonding between casing and cement may result in *microannulus*, a narrow gap or fracture that will serve as a conduit for formation fluids along the well. The resulting breach of well integrity would violate the zonal isolation requirement, necessitating expensive and cumbersome repair work [2].

When cement paste is poured into a container, the hydration process sets in [3]. Particles of tricalcium silicate (Ca_3SiO_5) are hydrated into calcium silicate hydrate, and thereby grow in size [4,5]. Interstitial water present in the cement paste is consumed in this process. Over time, cement sets, hardens, and turns into a porous solid material.

The hydraulic and mechanical bonding strength between a steel surface (e.g., container's walls) and hardened cement is affected by the structure and properties of a thin (20–100 μm thick) cement layer adjacent to the surface [6,7]. Such a layer between cement and another material (e.g., an aggregate particle) is known as the *interfacial transition zone* (ITZ) in cement literature [8]. Cement within the ITZ is typically more porous than both the bulk cement and the cement immediately adjacent to the wall [9]. As a result, failure at a cement-steel interface often takes place not at the very wall, but at some distance (on the order of 10 μm) into the cement [10]. Improving the shear and tensile strength at the interface must therefore be achievable through manipulating the structure of the ITZ.

One of the distinct features of ITZ is that it is depleted of large particles [8]. According to a geometry-based explanation of this phenomenon, if the packing of large cement particles were the same near the interface as in the bulk cement, the interface would have to cut through some of these particles. Since this is impossible, fewer large particles can be placed in the vicinity of a wall than in the bulk cement [8]. Another, physics-based explanation stipulates that large particles cannot approach the wall in the cement paste when cement is poured because the lubrication squeeze force prevents them from doing so [10,11]. The lubrication force increases indefinitely as the particle approaches the wall [12–14]. The viability of the lubrication-based hypothesis of ITZ formation was studied in recent experiments [11]. In particular, synchrotron μ-CT images of cement paste adjacent to a steel wall taken at the onset of hydration confirmed that the near-wall zone (ca. 20 μm) is depleted of large cement particles even before hydration starts.

Since cement particles are known to carry electric charge, it should be possible to use electrophoresis to control the packing of particles near the wall and thus the structure of the ITZ. Since the structure of the ITZ ultimately is likely to affect (at least some of) ITZ's properties, it seems to be a plausible conjecture that electric field could be used to control/alter the interface properties. Simple experiments confirmed that this indeed is the case [15]: Applying positive potential to a steel electrode immersed into a neat cement paste (neat cement is free of special additives used in oil-well cements) produced better cement-steel adhesion compared to a reference test without voltage. Applying negative potential produced an opposite effect, effectively cleaning the electrode.

Even though the above results indicate that electrophoresis could indeed be used to manipulate the ITZ structure and the cement-steel bonding, practical application of this technology requires that the mechanisms responsible for the observed phenomenon be well-understood first. In particular, the following fundamental question must be answered: How does the electric field affect the structure of the ITZ and, in particular, the *occurrence of large particles near the wall*? Answering this question was one of the objective of this study. Another objective was to supply a method capable of capturing and quantifying the structural changes within the interfacial transition zone.

2. Experiments

The cement slurry was prepared based on sulphate-resistant well cement from Norcem (Norway). Chemical composition of the cement supplied by the manufacturer is given in Table 1.

Table 1. Approximate chemical composition of the dry cement (according to supplier's specification).

Phase	Content in dry cement, %
C_3S (tricalcium silicate)	64.7
C_4AF (tetracalcium alumino ferrite)	17.5
C_3A (tricalcium aluminate)	1.3
MgO, SO_3, Na_2O, insoluble residues	4.4

The water-to-cement ratio was equal to 0.44. After the cement paste had been mixed, steel electrodes were inserted into it. Each electrode was a pipe 5 mm in diameter, with the wall thickness of 1 mm. Pipes were made of steel St 37.4 (Astrup, Norway). Voltage of 18 V was applied between the electrodes for 5 min. The cement was then left to harden for one day before the electrodes were pulled out of cement. After the electrodes had been removed, the cement block was locked in a closed container in order to avoid water evaporation during further curing for at least one month. High-resolution μ-CT scans of the near-wall region at anode and cathode were then performed. The measurements were done at beam-line TOMCAT at Swiss Light Source with energy of 22 keV. The 2D projections were obtained with the field of view of 1.7×1.4 mm^2, a pixel size of 0.65×0.65 μm^2, and a detector-sample distance of 125 mm. For the reconstruction of the phase-contrast 2D projections the ANKAphase program [16] was used to retrieve the phase and then to reconstruct. Segmentation and visualization were performed using the VGstudio program.

In order to quantify the structure of the near-wall zone near anode and cathode, smaller volumes of the total μ-CT image adjacent to the cement-steel interface were selected for particle size distribution (PSD) analyses. The volumes analysed for PSD were equal to $911 \times 841 \times 520$ μm^3 near cathode and $616 \times 364 \times 678$ μm^3 near anode (Figure 1). The areas shown in Figure 1 were selected as they represent the typical structure observed at cathode and anode.

The following data processing was employed for particle size distribution analysis [11]:

- Individual particles were identified from μ-CT images and highlighted in yellow (Figure 1). To this end, first an erosion filter was applied to the μ-CT image to enhance the contrast and to separate the particles. Then, the brightest particles were selected by applying a grayscale threshold.

- For each particle, two parameters were obtained from the µ-CT data: the particle's volume and the particle's distance to wall. Distance to wall was defined as the shortest distance from the particle's surface to the electrode's surface (Figure 2a).
- For each particle, the equivalent diameter was calculated (the diameter of a spherical particle having the same volume as the real particle).
- A threshold particle size was chosen (10 µm in this study). All particles smaller than the threshold size were classified as "small". All particles larger than the threshold were classified as "large".
- All particles were binned according to their distance from wall, i.e., particles having the gap from 0 to 10 µm, from 10 to 20 µm, from 20 to 30 µm, etc. (Figure 2b).
- The number of "small" particles and the number of "large" particles were calculated for each bin.
- The ratio of the two numbers, the number of large particles to the number of small particles, was calculated for each bin.
- This ratio was then plotted as a function of the bin distance from the wall. The bin distance was defined as the distance from the centre of the bin to the wall, i.e., 5 µm for the first bin, 15 µm for the second bin, etc. The interpretation of these plots is described in the next Section.

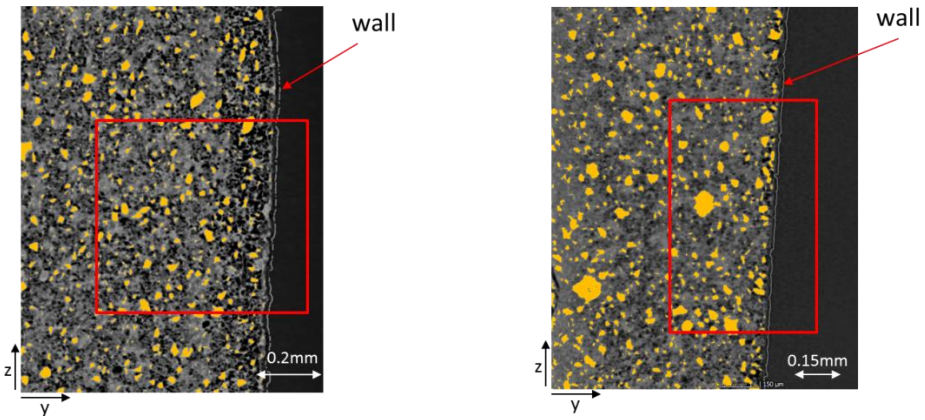

(a) (b)

Figure 1. Near-wall zone at cathode (a) and anode (b). The approximate areas chosen for particle size distribution analyses are indicated with red boxes.

(a) (b)

Figure 2. Definition of particle's distance to wall (a) and the binning procedure in particle size distribution analysis (b).

The choice of threshold particle size (10 μm) was made after several other thresholds were tried. It turned out that thresholds around and equal to 10 μm produce the best results.

In addition to PSD analyses, X-ray powder diffraction was employed to establish differences (if any) in chemical composition between the near-wall zones near cathode and anode. The analyses were performed on a Bruker D8 Advance Da Vinci diffractometer using CuKα radiation. The powder was obtained by scraping the surface of the cement which was in contact with the steel. The X-ray powder diffraction pattern were collected on the powder spread out on silicon substrate during 1 hour in the range between 5–75° 2θ angle.

3. Results and discussion

Differences in the structure of the near-wall area at cathode and anode could be observed even with the naked eye: The near-wall region in Figure 1a looks looser than the one in Figure 1b. Thus, the loose packing of cement particles characteristic of the ITZ is enhanced by applying negative potential to the wall. These structural changes might be the cause for poor cement-steel adhesion at the cathode reported in [15]. The ITZ near anode (Figure 1b) looks less loose. This is, most likely, the underlying mechanism for improved adhesion observed at anode [15].

Particle size distribution analyses near anode and cathode allowed us to quantify the width of the near-wall region where the structure is affected by electrophoresis. The number ratio of "large" to "small" particles obtained by the procedure described in the Experimental Section was found to decrease with the distance from anode (blue curve in Figure 3), while it increased with the distance from cathode (sandy brown curve in Figure 3). This implies that positive voltage increases the prevalence of large particles near the electrode, compared to the negative voltage. The zone of influence was found to stretch for approximately 40 μm from the wall (Figure 3). It is, however, conceivable that the width of the zone of influence could depend on the voltage, the zeta-potential of cement particles, and the composition and rheology of the interstitial fluid.

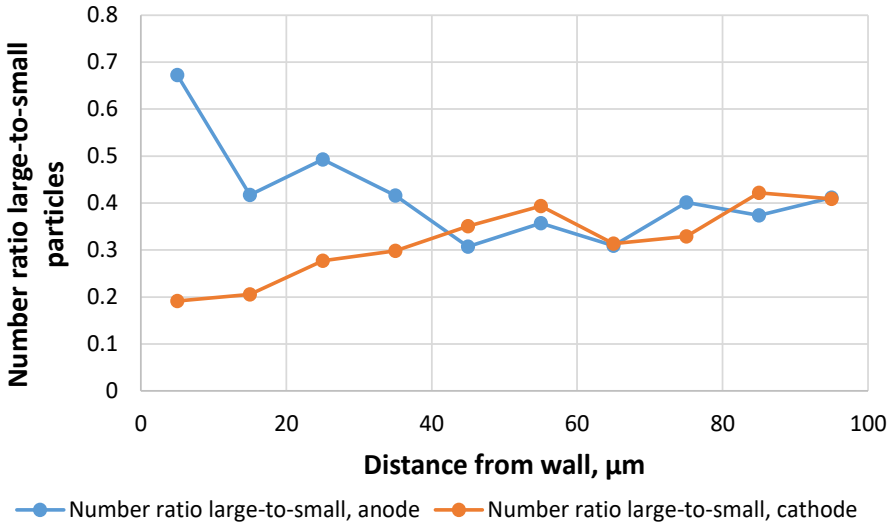

Figure 3. Number ration of "large" to "small" particles vs. distance to anode (blue curve) and cathode (sandy brown curve). "Large" and "small" particles have equivalent diameter greater than 10 μm and smaller than 10 μm, respectively.

The results are consistent with the experimental fact that cement particles in neat cement usually have negative zeta-potential [17]. The magnitude and sign of the zeta-potential can be altered by changing the ionic strength of the interstitial (carrier) fluid, the pH, and the shearing time of the cement paste [17–20]. Therefore, it is not necessarily positive potential that would improve the ITZ structure, and thus bonding, in all cases. What is clear, however, is that, given that cement particles have nonzero zeta-potential, the structure of the ITZ can be manipulated by applying voltage to wall. In particular, applying potential of the opposite sign (positive for particles with negative zeta-potential, negative otherwise) increases the presence of large particles in the ITZ. This, most likely, is the mechanism for the increased adhesion at anode observed in earlier experiments [15]. Applying electric potential of the same sign as the zeta-potential of cement particles renders the ITZ depleted of large particles, and thereby makes the particle packing in the ITZ looser. The cement-steel adhesion is thereby worsened. In future experiments, the bonding strength (shear and tensile) should be quantified by performing, e.g., pushout or rip-off tests, in order to confirm that better adhesion seen at anode also results in improved strength of the steel-cement interface after cement has hardened.

XRD analyses revealed that chemical composition of the ITZ was different near anode and cathode (Figure 4). Namely, the near-wall region at anode was enriched with tricalcium silicate (Ca_3SiO_5). Without providing a direct proof, this observation suggests that the large particles attracted towards anode were mainly composed of tricalcium silicate in our experiments. These largest tricalcium silicate particles present in the hardened cement are non-hydrated cement particles.

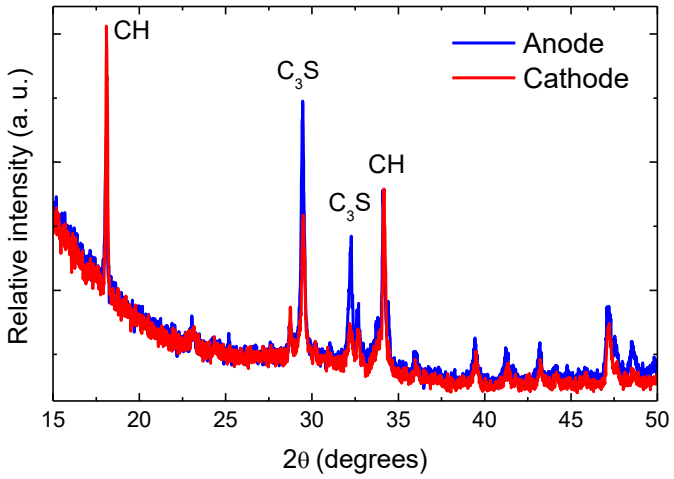

Figure 4. X-ray powder diffraction patterns of near-wall zones at cathode (red) and anode (blue). CH and C_3S are cement chemistry notations for calcium hydroxide $Ca(OH)_2$ and calcium silicate Ca_3SiO_5, respectively.

We cannot dismiss the possibility that the observed disproportion in the distribution of large non-hydrated particles near cathode and anode is a consequence of different cement hydration conditions close to the two electrodes. The electric-field-induced particle packing around the electrodes might be associated with perturbed water content near the electrodes compared to the bulk cement. Better particle packing close to the anode implies lower water content (water/cement ratio). This in turn may lead to a lower dissolution and hydration degree of the large tricalcium silicate

particles compared to the cement near cathode. Thus, the unreacted particles would be more abundant near anode.

4. Summary and conclusions

Electric field affects the particle size distribution near the electrodes immersed into a neat-cement paste. Positive field attracts large particles, which explains why better cement-steel adhesion has been observed at the positive electrode. The distance of influence of the electric field in our experiments (neat cement, voltage 18 V applied for 5 min) was approximately 40 μm. Given that the width of the ITZ in cement is typically 20–100 μm, this was enough to affect the structure of the ITZ. Chemical composition of the ITZ was affected by the electric field as well. In particular, the percentage of tricalcium silicate was elevated near anode.

These experiments suggest that electrophoresis-enhanced adhesion of cement to a steel wall discovered earlier [15] is due to larger particles being attracted to the electrode having the opposite polarity to cement particles' zeta-potential. This improves the packing and overall "quality" of the ITZ, making it less different from the surrounding bulk cement. This is observed macroscopically as improved cement adhesion to anode. Further research should address the effect of additives typically present in well cements. Additives are likely to affect the zeta-potential of cement particles and thereby the magnitude of the electrophoresis-induced structural changes.

Acknowledgments

This publication has been produced in the projects "Closing the gaps in CO_2 well plugging" (243765/E20) and "Voltage on casing for improved well cement quality" (267651/E20) funded by the Research Council of Norway through the CLIMIT and PETROMAKS2 programs. The authors are grateful to the Swiss Light Source for access to the TOMCAT beamline.

Conflict of interest

The authors declare no conflicts of interest regarding this paper.

References

1. Nelson EB, Guillot D (2006) *Well cementing*, Sugar Land: Schlumberger.
2. Kjøller C, Torsæter M, Lavrov A, et al. (2016) Novel experimental/numerical approach to evaluate the permeability of cement-caprock systems. *Int J Greenh Gas Con* 45: 86–93.
3. Bullard JW, Jennings HM, Livingston RA, et al. (2011) Mechanisms of cement hydration. *Cement Concrete Res* 41: 1208–1223.
4. Van Breugel K (1995) Numerical simulation of hydration and microstructural development in hardening cement-based materials (I) theory. *Cement Concrete Res* 25: 319–331.
5. Thomas JJ, Biernacki JJ, Bullard JW, et al. (2011) Modeling and simulation of cement hydration kinetics and microstructure development. *Cement Concrete Res* 41: 1257–1278.
6. Bentur A, Diamond S, Mindess S (1985) The microstructure of the steel fibre-cement interface. *J Mater Sci* 20: 3610–3620.

7. Zhu X, Gao Y, Dai Z, et al. (2018) Effect of interfacial transition zone on the Young's modulus of carbon nanofiber reinforced cement concrete. *Cement Concrete Res* 107: 49–63.
8. Scrivener KL, Crumbie AK, Laugesen P (2004) The Interfacial Transition Zone (ITZ) Between Cement Paste and Aggregate in Concrete. *Interf Sci* 12: 411–421.
9. Zhu W, Bartos PJM (2000) Application of depth-sensing microindentation testing to study of interfacial transition zone in reinforced concrete. *Cement Concrete Res* 30: 1299–1304.
10. Torsæter M, Todorovic J, Lavrov A (2015) Structure and debonding at cement–steel and cement–rock interfaces: Effect of geometry and materials. *Constr Build Mater* 96: 164–171.
11. Lavrov A, Panduro EAC, Torsæter M (2017) Synchrotron study of cement hydration: Towards computed tomography analysis of interfacial transition zone. *Energy Procedia* 114: 5109–5117.
12. Dance SL, Maxey MR (2003) Incorporation of lubrication effects into the force-coupling method for particulate two-phase flow. *J Comput Phys* 189: 212–238.
13. Kim S, Karrila SJ (2005) *Microhydrodynamics: principles and selected applications*, Mineola: Dover Publications.
14. Lavrov A, Laux H (2007) DEM modeling of particle restitution coefficient vs Stokes number: The role of lubrication force. 6th International Conference on Multiphase Flow, ICMF 2007, Leipzig, Germany.
15. Lavrov A, Gawel K, Torsæter M (2016) Manipulating cement-steel interface by means of electric field: Experiment and potential applications. *AIMS Mater Sci* 3: 1199–1207.
16. Weitkamp T, Haas D, Wegrzynek D, et al. (2011) ANKAphase: software for single-distance phase retrieval from inline X-ray phase-contrast radiographs. *J Synchrotron Radiat* 18: 617–629.
17. Hodne H, Saasen A (2000) The effect of the cement zeta potential and slurry conductivity on the consistency of oil-well cement slurries. *Cement Concrete Res* 30: 1767–1772.
18. Nachbaur L, Nkinamubanzi PC, Nonat A, et al. (1998) Electrokinetic properties which control the coagulation of silicate cement suspensions during early age hydration. *J Colloid Interf Sci* 202: 261–268.
19. Westermeier R (2016) *Electrophoresis in practice: a guide to methods and applications of DNA and protein separations*, John Wiley & Sons.
20. Yang M, Neubauer CM, Jennings HM (1997) Interparticle potential and sedimentation behavior of cement suspensions. *Adv Cement Based Mater* 5: 1–7.

AIMS Press